applied sciences

MDPI

Article

Fabrication of a Promising Hierarchical Porous Surface on Titanium for Promoting Biocompatibility

Wen-Chien Lan [1,2,†], Chia-Hsien Wang [3,†], Bai-Hung Huang [2,4,5], Yen-Chun Cho [6], Takashi Saito [7], Chien-Chia Huang [7] and Mao-Suan Huang [8,9,*]

1 Department of Oral Hygiene Care, Ching Kuo Institute of Management and Health, Keelung 203, Taiwan; jameslan@ems.cku.edu.tw
2 Biomedical Technology R & D Center, China Medical University Hospital, Taichung 404, Taiwan; babyfireh@gmail.com
3 Division of Family and Operative Dentistry, Department of Dentistry, Taipei Medical University Hospital, Taipei 110, Taiwan; dentintako@gmail.com
4 Asia Pacific Laser Institute, New Taipei City 220, Taiwan
5 Implant Academy of Minimally Invasive Dentistry, Taipei 106, Taiwan
6 School of Dentistry, Ceu Cardenal Herrera University, Valencia 46115, Spain; angel30923@hotmail.com
7 Division of Clinical Cariology and Endodontology, Department of Oral Rehabilitation, School of Dentistry, Health Sciences University of Hokkaido, Hokkaido 061-0293, Japan; t-saito@hoku-iryo-u.ac.jp (T.S.); courageev@hotmail.com (C.-C.H.)
8 Department of Dentistry, Taipei Medical University-Shuang Ho Hospital, New Taipei City 235, Taiwan
9 School of Oral Hygiene, College of Oral Medicine, Taipei Medical University, Taipei 110, Taiwan
* Correspondence: hms4837@tmu.edu.tw
† Co-first author: Chia-Hsien Wang.

Received: 12 November 2019; Accepted: 12 February 2020; Published: 17 February 2020

Abstract: The effects of the nano-titanium hydrides (nano-γ-TiH) phase on the formation of nanoporous Ti oxide layer by the potential approach (hydrogen fluoride (HF) pretreatment and sodium hydroxide (NaOH) anodization) were investigated using scanning electron microscopy, X-ray photoelectron spectroscopy, X-ray diffractometry, and transmission electron microscopy. The nano-γ-TiH phase was formed by the HF pretreatment with various current densities. After the NaOH anodization, the nano-γ-TiH phase was dissolved and transformed into nanoporous rutile-Ti dioxide (R-TiO_2). As the Ti underwent HF pretreatment and NaOH anodization, the microstructure on the surface layer was transformed from α-Ti → (α-Ti + nano-γ-TiH) → (α-Ti + R-TiO_2). In-vitro biocompatibility also indicated that the Ti with a hierarchical porous (micro and nanoporous) TiO_2 surface possessed great potential to enhance cell adhesion ability. Thus, the potential approach can be utilized to fabricate a promising hierarchical porous surface on the Ti implant for promoting biocompatibility.

Keywords: titanium oxide; titanium hydride; anodization; biocompatibility

1. Introduction

Metallic materials have been extensively applied in surgical implants [1–5]. Among them, titanium (Ti) and its alloys are widely adopted as metallic implants owing to their superior physical and chemical properties [6–15]. Ti and its alloys exhibit excellent corrosion (crevice corrosion and pitting) resistance. In addition, they are suitable for use in cooling water systems to clean polluted water. The excellent corrosion resistance of Ti and its alloys can be attributed to a dense oxide layer formation on their surface upon their exposure to atmospheric moisture [16–18]. This oxide film shows self-healing properties and is stable over a wide range of redox potentials. Moreover, the oxide layer is always present in

oxidizing media such as human body fluids and can be reconstituted within milliseconds after being damaged [19]. Ti-based alloys are also resistant to chemical species associated with micro-organisms such as nitrites, ammonium, sulfides, and organo-sulfur compounds. They are also resistant to acidic conditions and aerobic activity of microbes. Hence, Ti and its alloys are promising materials for medical implants.

The native oxide film also facilitates the adhesion and growth of micro and macro-foulants on the material surface. These microbes can form biofilms on the material surface and macro-organisms can improve the tissue healing efficiency of the implant material by reducing the healing time. However, amino acids and proteins in body fluids increase metal corrosion [20]. Ti-based alloys are not biotoxic. The release of metallic ions induces the osseo/osetointegration and often results in the clinical failure of metallic implants. Although the release of metallic ions is harmful, metallic implants are suitable for clinical applications owing to their high strength. However, the anti-corrosion performance and biocompatibility properties of metallic implants should be promoted. The presence of a Ti oxide layer on the Ti-based implants is considered a prerequisite for their biocompatibility. This Ti oxide film induces the formation and nucleation of apatite. In addition, the formation of a porous Ti oxide layer on the Ti implant [10] caused bone ingrowth into the porous structure, inducing the implant to be morphologically fixed to bones as compared with other porous nanomaterials [21,22].

Recently, various techniques—including thermal oxidation, anodization, and sol–gel methods—have been extensively used to investigate for the formation of Ti oxide layers [23,24]. Previous studies also reported that the formation of a nanoporous or hybrid porous (micro and nanoporous) Ti oxide layer on Ti surface not only enhanced cell adhesion and proliferation but also promoted the early stages of bone healing and osseointegration [10,25]. Based on the improvement of Ti dental implant, herein, we developed a potential approach (hydrogen fluoride (HF) pretreatment and sodium hydroxide (NaOH) anodization) to form a hierarchical porous (micro and nanoporous) Ti oxide surface. The surface properties, microstructural characteristics, and cellular behaviors of the treated Ti specimens were investigated for dental and biomedical applications.

2. Materials and Methods

2.1. Specimens Preparation

The thickness of 1 mm Ti sheet (ASTM F67 Grade II) was adopted as the substrate in this study. The specimen was prepared into discs with a diameter of 10 mm for carrying out the experiments. The specimens were ground and polished through a 1500 grit paper, diamond abrasives (particle size of 1 μm), and colloidal silica abrasives (particle size of 0.04 μm). Before conducting the experiments, the specimens were ultrasonically washed by acetone solution at 25 °C for 5 min. Then, the surface remained contaminates were further etched with a mixture solution of nitric acid (10%), hydrofluoric acid (2%), and ammonium fluoride (2%) at 25 °C for 1 min. Subsequently, the distilled water was used to wash the etched specimens by ultrasonic cleaning at 25 °C for 10 min. After the surface cleaning process, the pretreatments of HF polarization were performed in a solution of 1 M HF acid with different current densities (0.1 to 5 A/dm^2) for 10 min at 25 °C. Hereafter, the pretreated specimens were anodized in a solution contained with 5 M NaOH at 20 A/dm^2 for 10 min. For comparison, specimens without any treatment were also prepared as control group. The untreated Ti (control), HF-pretreated Ti, as well as HF-pretreated and anodized Ti specimens are labeled as Ti, HFP-Ti, and HFPA-Ti, respectively.

2.2. Surface Property Analysis

The topography features of the investigated specimens were examined through a JEOL JSM6400 scanning electron microscope (SEM; Tokyo, Japan) under a chamber pressure of 9.63×10^{-5} Pa and an operating voltage of 20 kV. The Perkin Elmer model PHI 1600 X-ray photoemission spectroscope (XPS; Waltham, MA, USA) was employed to analyze the chemical bonding states of the investigated specimens

with a radiation source of monochromatic Mg Kα under 15 kV, 16.7 mA, and 250 W. The binding energy of the Ag 3d5/2 line on clean Ag was used to calibrate the XPS level. The incident angle of the X-ray beam to the specimen normal was 45°. The X-ray beam with a diameter of ~15 nm was used to detect the surface elements by high-resolution scans. Before analysis, the spectrum was curve-fitted with a Gaussian–Lorentzian peak. The phase compositions of the investigated specimens were identified via Rigaku 2200 thin film X-ray diffractometer (TF-XRD; Tokyo, Japan) with an incident angle (Cu Kα radiation) of 3° at 50 kV and 250 mA. Moreover, the JEOL-2100 high-resolution transmission electron microscope (TEM; Tokyo, Japan) was also employed to examine the microstructures of the investigated specimens. For the cross-sectional observation of TEM, electron-transparent samples were prepared using mechanical thinning and argon ion milling.

2.3. In Vitro Biocompatibility Testing

The investigated specimens were subjected to cell culture in order to evaluate the cell reactions (proliferation and adhesion behaviors). Before carrying out the biocompatibility testing, the investigated samples were sterilized using the 3 M 8 XL ethylene oxide sterilizer (Saint Paul, MN, USA). Hereafter, the investigated specimens were placed into the 24-well polystyrene plate. The Dulbecco's modified Eagle's medium (Gibco, Waltham, MA, USA) containing fetal bovine serum (10%), streptomycin (100 mg/mL), and penicillin (100 units/mL) was used as the culture medium of osteoblast-like cells (MG-63). The cell suspension with a density of 1 × 104 per 100 μL was added to each well. Subsequently, the cell-seeded specimens were incubated at 37 °C for 1, 3, 5, and 7 days in a humidified atmosphere of 95% air and 5% CO_2, respectively. Finally, the cells on the cultured specimens were evaluated through SEM at different magnifications to observe their adhesion morphology and proliferation characteristics.

3. Results and Discussion

3.1. Surface Characterizations

Figure 1 illustrates the SEM micrographs of the investigated specimens (Ti, HFP-Ti at 1 A/dm^2 for 10 min, and HFPA-Ti). It can be observed from Figure 1a, the surface of Ti exhibited clear machined tracks. Figure 1b shows the surface of the HFP-Ti (1 A/dm^2 for 10 min) specimen with a large number of micropores (as indicated by white arrows) and microcracks (as indicated by black arrows). The number of micropores and microcracks increased as the pretreatment current density increasing. The surface of the HFPA-Ti specimen became microporous topography as shown in Figure 1c. However, it was found that the presence of nanoporous structure can be observed from a higher magnification SEM micrograph (Figure 1d). This feature can also be discovered in the other HFPA-Ti specimens with different pretreatment current densities. Accordingly, the formation of a hierarchical porous (micro and nanoporous) surface as the Ti modified with HF pretreatment and NaOH anodization. The porous structure can usually be obtained by immersing the implant in an alkaline solution for a long time [26]. Microcracks are generated by the microdefect and/or oxidation effects. It is well-known that Ti implants with nanoporous surface exhibit excellent performance because of the enhanced cell adhesion and differentiation between the implant and genuine bones [10,27].

Figure 2 presents the regional scans of O 1 s peaks taken from the investigated specimens (Ti, HFP-Ti at 2 A/dm^2 for 10 min, and HFPA-Ti). The Ti specimen showed chemical bonding states corresponding to O. The O 1 s peak of Ti was formed at 531 eV. A similar tendency at 531 eV can also be observed in the HFP-Ti specimen (2 A/dm^2 for 10 min). The results reveal that certain of O atoms did not bond with Ti atoms during the HF pretreatments. However, the O 1 s peak shifted to ~530 eV in the case of the HFPA-Ti specimen. This finding indicates that the O atoms did bond with Ti atoms during the anodization treatment. Most of the O reacts with the Ti through diffusion when all the Ti atoms are oxidized. This exothermic reaction induces O atoms fixed at lattice or interstitial sites. It generates a crucial driving force for transporting O atoms or other species (O_2, O*, and O^{2-}) from the TiOx/Ti interface towards the TiO_2/Ti [28]. Similar results have been reported by Kim et al. [27]. Therefore,

the analytical results indicate that the anodization treatment induces a formation of the oxide layer on the surfaces of the HFPA-Ti specimens.

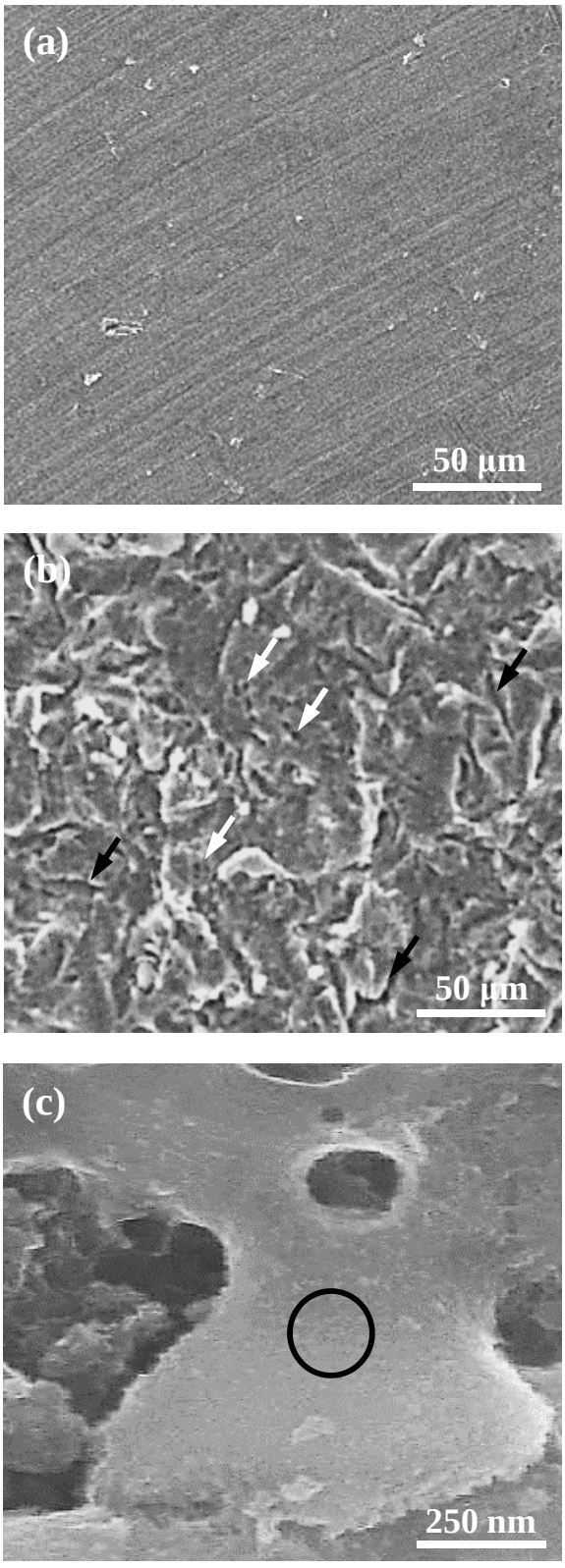

Figure 1. *Cont.*

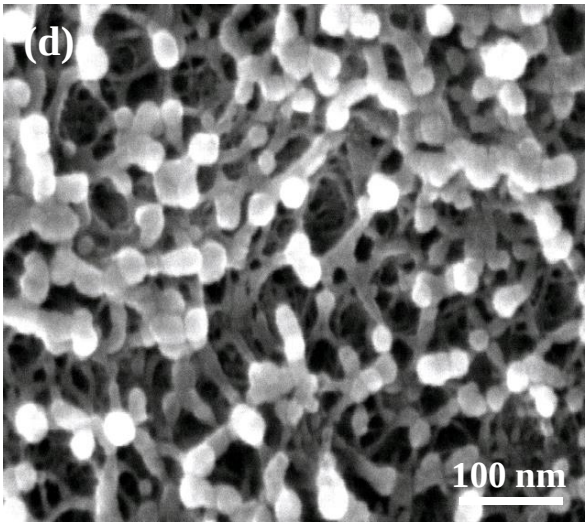

Figure 1. The SEM micrographs of the investigated specimens: (**a**) Ti, (**b**) HFP-Ti at 1 A/dm^2 for 10 min, (**c**) HFPA-Ti, and (**d**) a higher magnification image taken from the black circle area in (**c**).

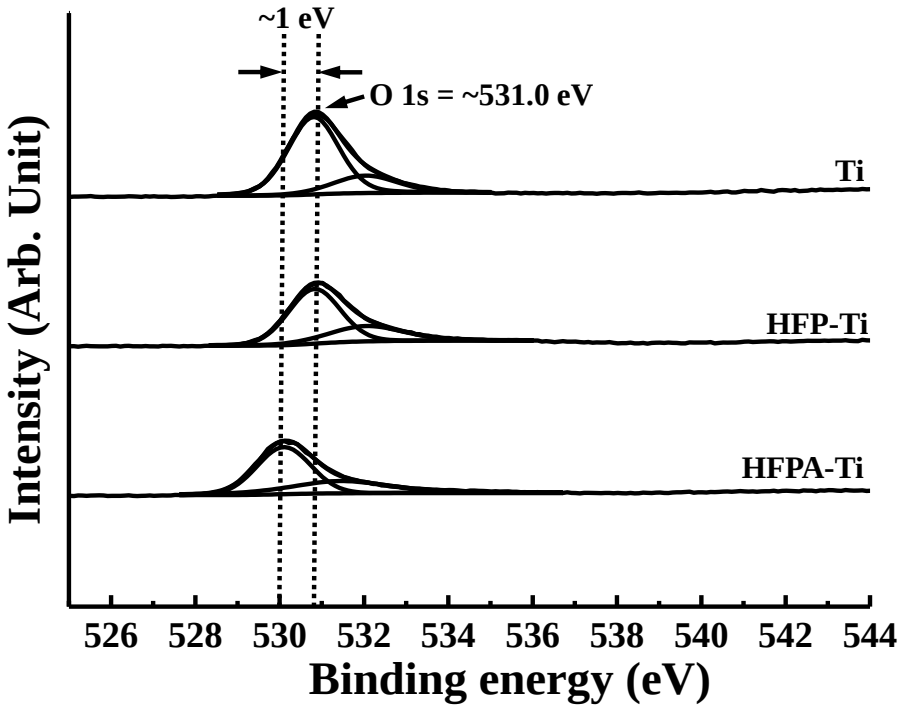

Figure 2. The regional scans of O 1 s peaks taken from the investigated specimens (Ti, HFP-Ti at 2 A/dm^2 for 10 min, and HFPA-Ti).

3.2. Microstructural Variations

Figure 3 displays the TF-XRD patterns of the investigated specimens (Ti, HFP-Ti at 2 A/dm^2 for 10 min, and HFPA-Ti). In the case of the Ti specimen, only the reflection peaks of α-Ti phase with hexagonal close-packed crystal structure were clearly detected. While the HFP-Ti specimen (2 A/dm^2 for 10 min) showed the additional reflection peaks. Based on the database from the Joint Committee on Powder Diffraction Stand, it was found that the additional reflection peaks belong to the Ti hydrides (γ-TiH) phase with tetragonal structure. A similar diffraction pattern can also be detected from those HFP-Ti specimens with different pretreatment current densities. Thus, the HFP-Ti specimens were consisted of α-Ti phase and γ-TiH phase. After the anodization treatment, the reflection peaks of

rutile-Ti dioxide (R-TiO_2) were formed on all of the HFPA-Ti specimens. Figure 4 shows the dark-field TEM micrograph of nano-particle taken from the surface layer of the HFP-Ti specimen at 1 A/dm^2 for 10 min. The d-spacings and camera length of the reflection spots indicated that the nano-particle is the γ-TiH phase having a tetragonal structure and lattice constant =0.434 nm. Accordingly, the results demonstrate that when the Ti underwent HF pretreatment and NaOH anodization, the microstructure on the surface layer was transformed from α-Ti → (α-Ti + nano-γ-TiH) → (α-Ti + R-TiO_2).

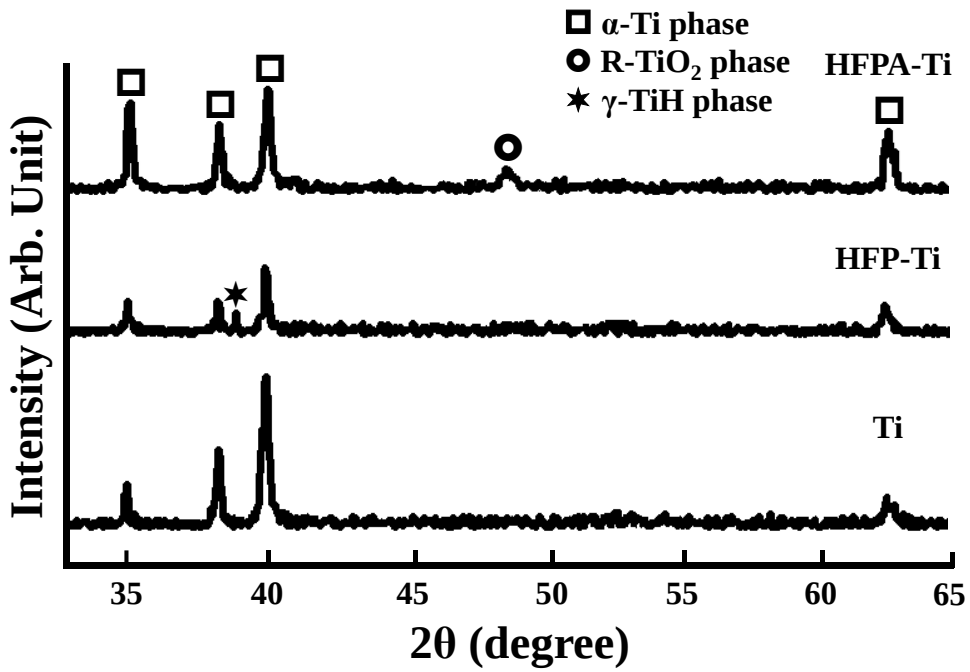

Figure 3. TF-XRD patterns of the investigated specimens (Ti, HFP-Ti at 2 A/dm^2 for 10 min, and HFPA-Ti).

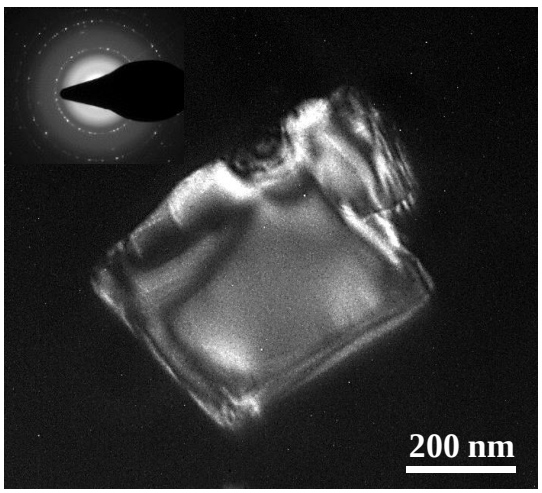

Figure 4. Dark-field TEM micrograph of nano-particle taken from the surface layer of the HFP-Ti specimen at 1 A/dm^2 for 10 min.

3.3. Cellular Behaviors

Figure 5 depicts the SEM micrographs of MG-63 cells on the investigated specimens after cultured with 1 day. The cells appear in a spindle-like shape and the centrally protruding nuclei were surrounded by thin cytoplasmic edges on the Ti specimen as shown in Figure 5a. As the incubation period increasing, it was found that the cells have almost completely adhered to the specimen surface. A similar cell

adhesion behavior can also be observed on the HFP-Ti specimens with different pretreatment current densities. As the HFPA-Ti specimen underwent an incubation of 1 day (Figure 5b), it is clearly seen that the cells exhibited good adhesion behavior with numerous filopodia (as indicated by black arrows) on the nanoporous surface from a higher magnification observation. The filopodia of cells tightly grabbed the nanoporous surface in comparison to the cells only adhered to the Ti and HFP-Ti specimens. This characteristic of cell adhesion behavior can also be found on the investigated specimens with a longer incubation period. Therefore, it is evident that the HFPA-Ti specimen possessed great potential to enhance cell adhesion ability.

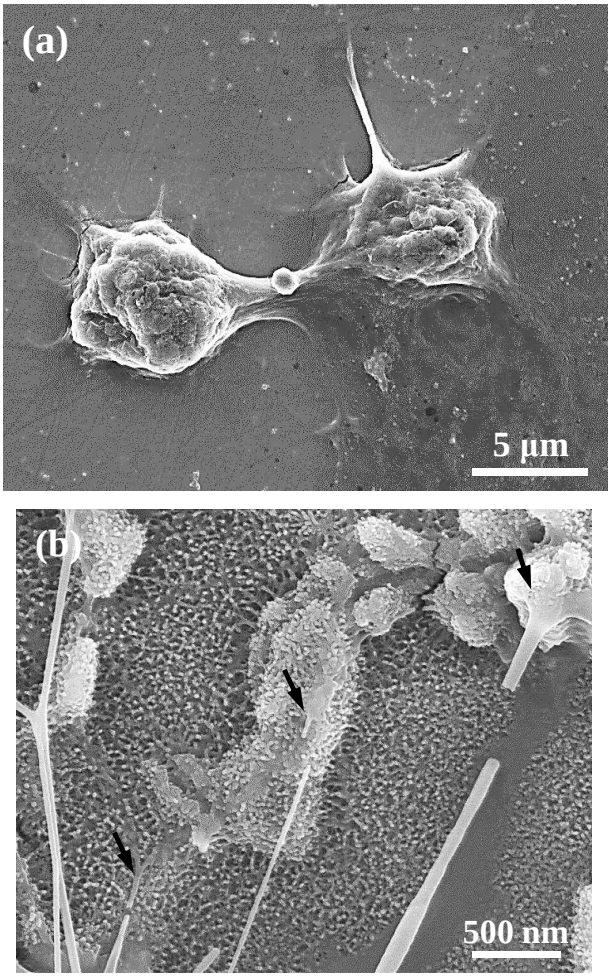

Figure 5. SEM micrographs of MG-63 cells on the investigated specimens after cultured with 1 day: (**a**) Ti and (**b**) HFPA-Ti.

It is well-known that hydrogen penetrated the samples during their mechanical polishing or chemical etching [29]. Hydrogen was also detected on the subsurface of the mirror-polished and sandblasted (with large grit and acid (SLA)) samples [30]. In the present study, the HFP-Ti specimens exhibited the hydrogen reaction and/or penetration. Hydrogen existed on the surface, and the concentration of hydrogen increased by increasing current density. The amount of hydrogen increased for the formation of a large number of nano-γ-TiH. Hence, the surface formed an oxide layer with microporous structure, as shown in Figure 1b. While the oxide layer acted as the barrier layer for hydrogen diffusion and blocked the hydrogen desorption. The ability of the oxide layer to block the metal ions diffusion can be promoted by raising the oxide thickness through surface treatment. As the Ti oxide layer thickness increased, the adsorption ratio of albumin/fibrinogen of Ti enhanced by six times [31]. However, the HFPA-Ti surface layer showed a hierarchical porous (micro and nanoporous)

surface as shown in Figure 1c,d. The formation of the hierarchical porous surface could be attributed that the hydrogen absorption and charging in the HF pretreatment caused the α-Ti to nano-γ-TiH transformation. After the formation of nano-γ-TiH, nanopores are generated by anodization to dissolve nano-γ-TiH. The formation of the nano-γ-TiH phase or the hydrogen absorption is essential to produce a nanoporous TiO_2 layer after the anodization treatment. Moreover, the anodization treatment results in the variation of enthalpy ($\Delta H > 0$). The elevated electrolyte temperature is beneficial to the reactants. An increase in the electrolyte temperature inhibits the oxide films formation. This is because of a controllable anodized oxide films thickness [32]. The oxide layer formation can mainly be attributed to redox reactions. The hydrogen reaction and penetration cause the nano-γ-TiH formation. It is believed that the nanophases dissolution is crucial for the nanoporous Ti oxide layer formation. Thus, Ti implants with a hierarchical porous (micro and nanoporous) TiO_2 surface can promote cell adhesion, thereby enhancing the bone cell ingrowth into the nanoporous structure, which provided the mechanical fixation of the implant to the bone.

4. Conclusions

The Ti subjected to the HF pretreatment with different current densities showed the formation of the nano-γ-TiH phase, which acted as a sacrificial precipitate. After the anodization treatment, the hierarchical porous (micro and nanoporous) TiO_2 surface was formed because of the nano-γ-TiH dissolution. An in vitro assessment also demonstrated that the HFPA-Ti specimen possessed great potential to enhance cell adhesion ability. Therefore, the process (HF pretreatment and NaOH anodization) is a promising approach for generating a biofunctional surface for dental Ti implant applications.

Author Contributions: Investigation and Writing—original draft, W.-C.L.; Project administration, B.-H.H.; Data curation, Y.-C.C.; Conceptualization, T.S.; Validation, C.-C.H.; Writing—review and editing, C.-H.W. and M.-S.H. All authors have read and agreed to the published version of the manuscript.

Funding: This research received no external funding.

Conflicts of Interest: The authors report no conflicts of interest in this work.

References

1. Costa, B.C.; Tokuhara, C.K.; Rocha, L.A.; Oliveira, R.C.; Lisboa-Filho, P.N.; Pessoa, J.C. Vanadium ionic species from degradation of Ti-6Al-4V metallic implants: In vitro cytotoxicity and speciation evaluation. *Mater. Sci. Eng. C Mater. Biol. Appl.* **2019**, *96*, 730–739. [CrossRef] [PubMed]
2. Gomes, C.C.; Moreira, L.M.; Santos, V.J.S.V.; Ramos, A.S.; Lyon, J.P.; Soares, C.P.; Santos, F.V. Assessment of the genetic risks of a metallic alloy used in medical implants. *Genet. Mol. Biol.* **2011**, *34*, 116–121. [CrossRef] [PubMed]
3. Zhu, L.B.; Hu, D.Y.; Wang, Q.; Hou, J.; Li, M. Diffuse polymorphic eosinophilic cellulitis in a patient with metallic alloy implants: A possible association? *Int. J. Dermatol.* **2011**, *50*, 1535–1537. [CrossRef] [PubMed]
4. Fan, J.; Qiu, X.; Niu, X.D.; Tian, Z.; Sun, W.; Liu, X.J.; Li, Y.D.; Li, W.R.; Meng, J. Microstructure, mechanical properties, in vitro degradation and cytotoxicity evaluations of Mg-1.5Y-1.2Zn-0.44Zr alloys for biodegradable metallic implants. *Mat. Sci. Eng. C-Mater.* **2013**, *33*, 2345–2352. [CrossRef] [PubMed]
5. Bodelon, O.G.; Iglesias, C.; Garrido, J.; Clemente, C.; Garcia-Alonso, M.C.; Escudero, M.L. Analysis of metallic traces from the biodegradation of endomedullary AZ31 alloy temporary implants in rat organs after long implantation times. *Biomed. Mater.* **2015**, *10*, 045015. [CrossRef] [PubMed]
6. Da Rocha, S.S.; Adabo, G.L.; Vaz, L.G.; Henriques, G.E.P. Effect of thermal treatments on tensile strength of commercially cast pure titanium and Ti-6Al-4V alloys. *J. Mater. Sci.-Mater. Med.* **2005**, *16*, 759–766. [CrossRef]
7. Wu, C.M.; Peng, P.W.; Chou, H.H.; Ou, K.L.; Sugiatno, E.; Liu, C.M.; Huang, C.F. Microstructural, mechanical and biological characterizations of the promising titanium-tantalum alloy for biomedical applications. *J. Alloys Compd.* **2018**, *735*, 2604–2610. [CrossRef]

8. Bahl, S.; Das, S.; Suwas, S.; Chatterjee, K. Engineering the next-generation tin containing beta titanium alloys with high strength and low modulus for orthopedic applications. *J. Mech. Behav. Biomed. Mater.* **2018**, *78*, 124–133. [CrossRef]
9. Kopova, I.; Strasky, J.; Harcuba, P.; Landa, M.; Janecek, M.; Bacakova, L. Newly developed Ti-Nb-Zr-Ta-Si-Fe biomedical beta titanium alloys with increased strength and enhanced biocompatibility. *Mater. Sci. Eng. C Mater. Biol. Appl.* **2016**, *60*, 230–238. [CrossRef]
10. Hou, P.J.; Ou, K.L.; Wang, C.C.; Huang, C.F.; Ruslin, M.; Sugiatno, E.; Yang, T.S.; Chou, H.H. Hybrid micro/nanostructural surface offering improved stress distribution and enhanced osseointegration properties of the biomedical titanium implant. *J. Mech. Behav. Biomed. Mater.* **2018**, *79*, 173–180. [CrossRef]
11. Ou, K.L.; Weng, C.C.; Lin, Y.H.; Huang, M.S. A promising of alloying modified beta-type Titanium-Niobium implant for biomedical applications: Microstructural characteristics, in vitro biocompatibility and antibacterial performance. *J. Alloys Compd.* **2017**, *697*, 231–238. [CrossRef]
12. Szewczenko, J.; Marciniak, J.; Kajzer, W.; Kajzer, A. Evaluation of Corrosion Resistance of Titanium Alloys Used for Medical Implants. *Arch. Metall. Mater.* **2016**, *61*, 695–699. [CrossRef]
13. Zhou, S.X.; Wang, J.; Cai, P. Corrosion Resistance Investigation of Titanium Alloy as Tissue Engineered Bone Implant. *Int. J. Electrochem. Sci.* **2017**, *12*, 7174–7182. [CrossRef]
14. Mohan, L.; Raja, M.D.; Uma, T.S.; Rajendran, N.; Anandan, C. In-Vitro Biocompatibility Studies of Plasma-Nitrided Titanium Alloy beta-21S Using Fibroblast Cells. *J. Mater. Eng. Perform.* **2016**, *25*, 1508–1514. [CrossRef]
15. Markhoff, J.; Krogull, M.; Schulze, C.; Rotsch, C.; Hunger, S.; Bader, R. Biocompatibility and Inflammatory Potential of Titanium Alloys Cultivated with Human Osteoblasts, Fibroblasts and Macrophages. *Materials* **2017**, *10*, 52. [CrossRef] [PubMed]
16. Kaur, M.; Singh, K. Review on titanium and titanium based alloys as biomaterials for orthopaedic applications. *Mater. Sci. Eng. C-Mater.* **2019**, *102*, 844–862. [CrossRef]
17. Lopez, M.F.; Jimenez, J.A.; Gutierrez, A. XPS characterization of surface modified titanium alloys for use as biomaterials. *Vacuum* **2011**, *85*, 1076–1079. [CrossRef]
18. Vasilescu, M.; Dobrescu, M. Titanium and Titanium Alloys as Biomaterials. Properties, Processing and Dental Applications. *Metal. Int.* **2010**, *15*, 69–73.
19. Cheng, H.C.; Lee, S.Y.; Chen, C.C.; Shyng, Y.C.; Ou, K.L. Influence of hydrogen charging on the formation of nanostructural titania by anodizing with cathodic pretreatment. *J. Electrochem. Soc.* **2007**, *154*, E13–E18. [CrossRef]
20. Eliaz, N. Corrosion of Metallic Biomaterials: A Review. *Materials* **2019**, *12*, 16. [CrossRef]
21. Shin, Y.C.; Pang, K.M.; Han, D.W.; Lee, K.H.; Ha, Y.C.; Park, J.W.; Kim, B.; Kim, D.; Lee, J.H. Enhanced osteogenic differentiation of human mesenchymal stem cells on Ti surfaces with electrochemical nanopattern formation. *Mater. Sci. Eng. C-Mater.* **2019**, *99*, 1174–1181. [CrossRef] [PubMed]
22. Suganya, P.; Venkadesh, A.; Mathiyarasu, J.; Radhakrishnan, S. MOF assisted synthesis of new porous nickel phosphate nanorods as an advanced electrode material for energy storage application. *J. Solid. State Electr.* **2019**, *23*, 3429–3435. [CrossRef]
23. Yetim, A.F. Investigation of wear behavior of titanium oxide films, produced by anodic oxidation, on commercially pure titanium in vacuum conditions. *Surf. Coat. Technol.* **2010**, *205*, 1757–1763. [CrossRef]
24. Velten, D.; Biehl, V.; Aubertin, F.; Valeske, B.; Possart, W.; Breme, J. Preparation of TiO_2 layers on cp-Ti and Ti6Al4V by thermal and anodic oxidation and by sol-gel coating techniques and their characterization. *J. Biomed. Mater. Res.* **2002**, *59*, 18–28. [CrossRef] [PubMed]
25. Tsai, M.H.; Haung, C.F.; Shyu, S.S.; Chou, Y.R.; Lin, M.H.; Peng, P.W.; Ou, K.L.; Yu, C.H. Surface modification induced phase transformation and structure variation on the rapidly solidified recast layer of titanium. *Mater. Charact.* **2015**, *106*, 463–469. [CrossRef]
26. Tanaka, S.; Aonuma, M.; Hirose, N.; Tanaki, T. The preparation of porous TiO_2 by immersing Ti in NaOH solution. *J. Electrochem. Soc.* **2002**, *149*, D167–D171. [CrossRef]
27. Kim, K.; Lee, B.A.; Piao, X.H.; Chung, H.J.; Kim, Y.J. Surface characteristics and bioactivity of an anodized titanium surface. *J. Periodontal. Implant Sci.* **2013**, *43*, 198–205. [CrossRef]
28. HChiang, J.; Chou, H.H.; Ou, K.L.; Sugiatno, E.; Ruslin, M.; Waris, R.A.; Huang, C.F.; Liu, C.M.; Peng, P.W. Evaluation of Surface Characteristics and Hemocompatibility on the Oxygen Plasma-Modified Biomedical Titanium. *Metals* **2018**, *8*, 513. [CrossRef]

29. Tanaka, S.; Iwatani, T.; Hirose, N.; Tanaki, T. Effect of hydrogen on the formation of porous TiO_2 in alkaline solution. *J. Electrochem. Soc.* **2002**, *149*, F186–F190. [CrossRef]
30. Taborelli, M.; Jobin, M.; Francois, P.; Vaudaux, P.; Tonetti, M.; Szmukler-Moncler, S.; Simpson, J.P.; Descouts, P. Influence of surface treatments developed for oral implants on the physical and biological properties of titanium. (I) Surface characterization. *Clin. Oral. Implants Res.* **1997**, *8*, 208–216. [CrossRef]
31. Sul, Y.T.; Johansson, C.B.; Jeong, Y.; Albrektsson, T. The electrochemical oxide growth behaviour on titanium in acid and alkaline electrolytes. *Med. Eng. Phys.* **2001**, *23*, 329–346. [CrossRef]
32. Sunny, M.C.; Sharma, C.P. Titanium-protein interaction: Changes with oxide layer thickness. *J. Biomater. Appl.* **1991**, *6*, 89–98. [CrossRef] [PubMed]